Magnetic induction mapping of magnetite chains in magnetotactic bacteria at room temperature and close to the Verwey transition using electron holography

E T Simpson[1,6], **T Kasama**[2,1]**, M Pósfai**[3]**, P R Buseck**[4]**, R J Harrison**[5] **and R E Dunin-Borkowski**[1,2]

[1] Department of Materials Science and Metallurgy, University of Cambridge, Pembroke Street, Cambridge CB2 3QZ, UK

[2] Frontier Research System, The Institute of Physical and Chemical Research, Hatoyama, Saitama 350-0395, Japan

[3] Department of Earth and Environmental Sciences, University of Veszprém, POB158, H-8201, Hungary

[4] Departments of Geological Sciences and Chemistry/Biochemistry, Arizona State University, Tempe, AZ 85287-1404, USA

[5] Department of Earth Sciences, University of Cambridge, Downing Street, Cambridge CB2 3EQ, UK

E-mail: ets22@cam.ac.uk

Abstract. Off-axis electron holography in the transmission electron microscope is used to record magnetic induction maps of closely spaced magnetite crystals in magnetotactic bacteria at room temperature and after cooling the sample using liquid nitrogen. The magnetic microstructure is related to the morphology and crystallography of the particles, and to interparticle interactions. At room temperature, the magnetic signal is dominated by interactions and shape anisotropy, with highly parallel and straight field lines following the axis of each chain of crystals closely. In contrast, at low temperature the magnetic induction undulates along the length of the chain. This behaviour may result from a competition between interparticle interactions and an easy axis of magnetisation that is no longer parallel to the chain axis. The quantitative nature of electron holography also allows the change in magnetisation in the crystals with temperature to be measured.

1. Introduction

The magnetic properties of arrangements of closely spaced magnetic nanoparticles result from a delicate balance between the competing effects of particle size, morphology, crystallography and spacing, and external factors such as temperature and applied magnetic field. Linear chains of ferrimagnetic magnetite crystals in magnetotactic bacteria provide a model system for studying the fundamental effects that influence the magnetic properties of closely spaced nanoscale magnets.

Here, we use off-axis electron holography in the transmission electron microscope (TEM) to image the magnetic induction in chains of biogenic magnetite nanocrystals from magnetotactic bacteria, both at room temperature and cooled using liquid nitrogen to a temperature close to the Verwey transition

---

[6] To whom any correspondence should be addressed

(119 K) in magnetite [1,2]. At this temperature, magnetite undergoes a phase change from a cubic to a monoclinic structure, and the size of the magnetocrystalline anisotropy increases markedly. This is accompanied by a change in the easy axis of magnetisation below a temperature of 130 K, the isotropic point, and we examine the effect of this transition on the magnetic induction in the crystals. Although bacterial cells do not naturally experience the temperatures and magnetic fields applied in these experiments, it is the mineral magnetic properties that are of primary interest in the present study rather than the biological importance of the magnetic properties of the crystals to the bacteria in their natural environment.

2. Experimental method, results and discussion

2.1 Sample background and preparation

A glass container was filled with sediment and water from Séd stream in Veszprém, Hungary, in the spring of 2000 and stored in dim light at room temperature. Magnetotactic bacteria were enriched by placing the magnetic south pole of a bar magnet next to the sediment/water interface, where the oxic/anoxic transition zone was expected. TEM samples were prepared by placing a drop that contained a large number of bacteria onto Formvar or carbon-coated Cu TEM grids.

A bright-field image of a representative cell, which contains two double chains of magnetite crystals, is shown in figure 1. The largest crystals are approximately 80 nm in length and 70 nm in width. Smaller, presumably more recently nucleated crystals are present at one or both ends of each magnetosome chain.

Figure 1. Bright-field image of a bacterial cell from Séd stream containing two double chains of magnetite magnetosomes, acquired at 400 kV using a JEOL 4000EX TEM. Crystals with darker contrast are more closely aligned to low-index zone axes.

Figure 2a shows a higher magnification bright-field image acquired from a similar cell. The particles are slightly elongated, and some of their corners appear to be rounded. Adjacent crystals are spaced approximately 5-10 nm apart, whereas the two parallel chains are separated by approximately 30 nm. In each crystal, the [111] axis is approximately parallel to the chain axis (see below). Slightly defocused images of other cells are shown in figures 2b and c. The smaller crystals at the ends of the chains are typically misoriented crystallographically with respect to the larger crystals.
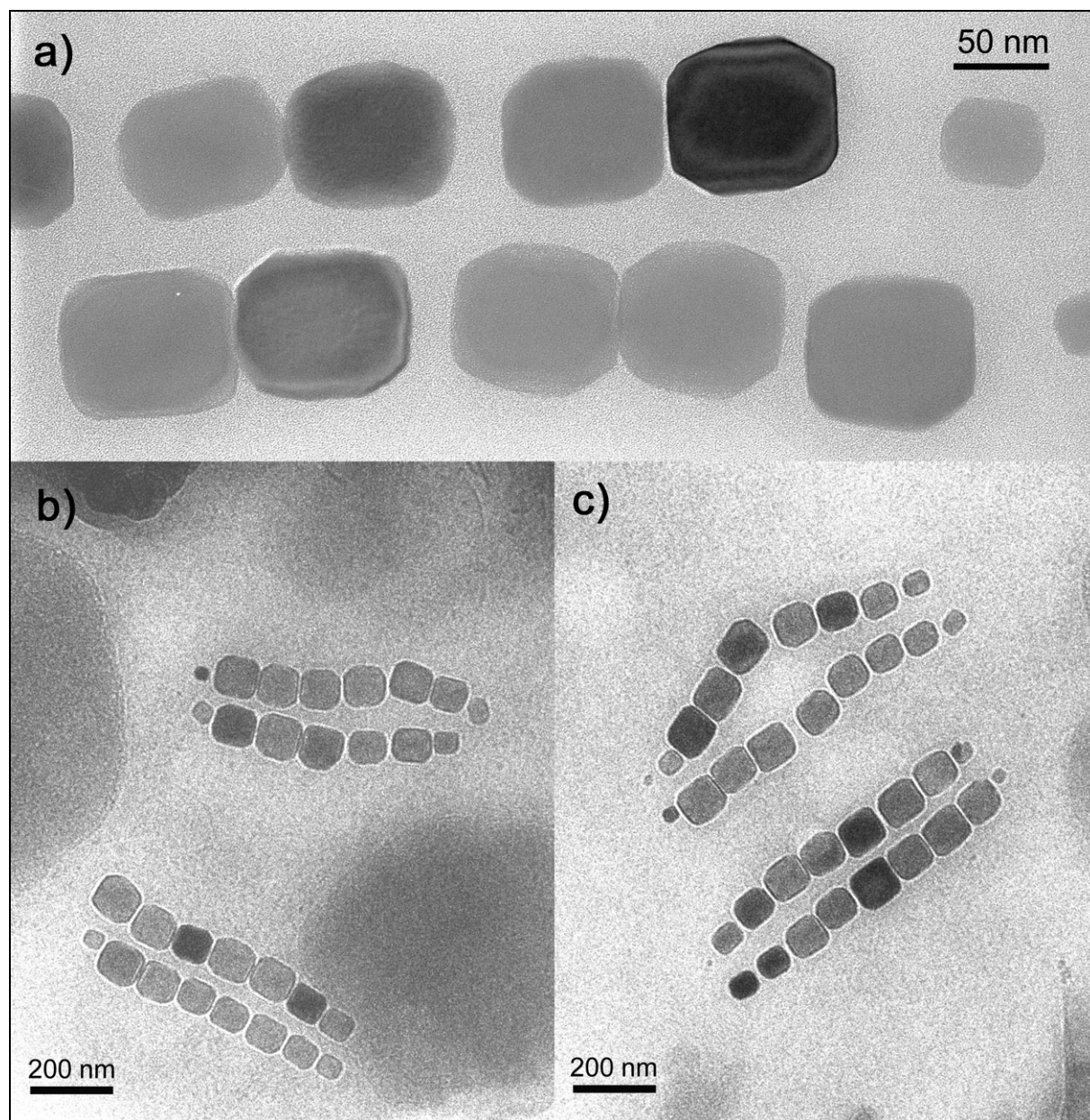
Figure 2. Bright-field images of magnetite chains in cells similar to that shown in figure 1. a) was recorded at 400 kV using a JEOL 4000EX TEM. b) and c) were recorded slightly underfocus at 300 kV using a Philips CM300 TEM, prior to acquiring electron holograms from the same regions (see below).

2.2 High-resolution electron microscopy

Information about the relative orientations of the magnetosomes in a single chain can be obtained from either zone-axis selected area electron diffraction (SAED) patterns or high-resolution (HR) images of individual crystals. Figure 3 shows a bright-field image of a double chain of magnetite crystals. By inspection, and with reference to previous literature on magnetite magnetosomes [3], apart from the crystals at the ends of the chains, [111] is nearly parallel to the chain axis in all of the magnetosomes, as indicated by the line of white arrows.

Figures 4 and 5 show zone-axis HR images and SAED patterns acquired from crystals 4 and 7, respectively. One of the tilt axes of the double-tilt specimen holder (y) was approximately parallel to the chain axis, while the other (x) was perpendicular to it. The small tilts about x that were required to achieve zone axis orientations in crystals 3-7 from a zone axis orientation in crystal 2 suggest that their [111] directions are approximately parallel to one another (and to the chain axis), the largest difference being 4.5° between crystals 3 and 7. In contrast, much larger tilt angles were required about y to achieve zone axis orientations. The measured crystal orientations (relative to crystal 2) are plotted on a stereogram in figure 6, which highlights this difference. Assuming that sample preparation has not altered the relative orientations of the crystals, the chain is therefore analogous to beads on a string that are allowed to rotate freely. Biological control over the orientations of the crystals appears to be stricter in setting [111] parallel to the chain axis than in constraining their orientation about this direction.

From a magnetic perspective, the alignment of the crystals ensures that their magnetocrystalline easy axes are closely parallel to the chain axis at room temperature. However, this relationship no longer holds below the Verwey transition, as discussed below.
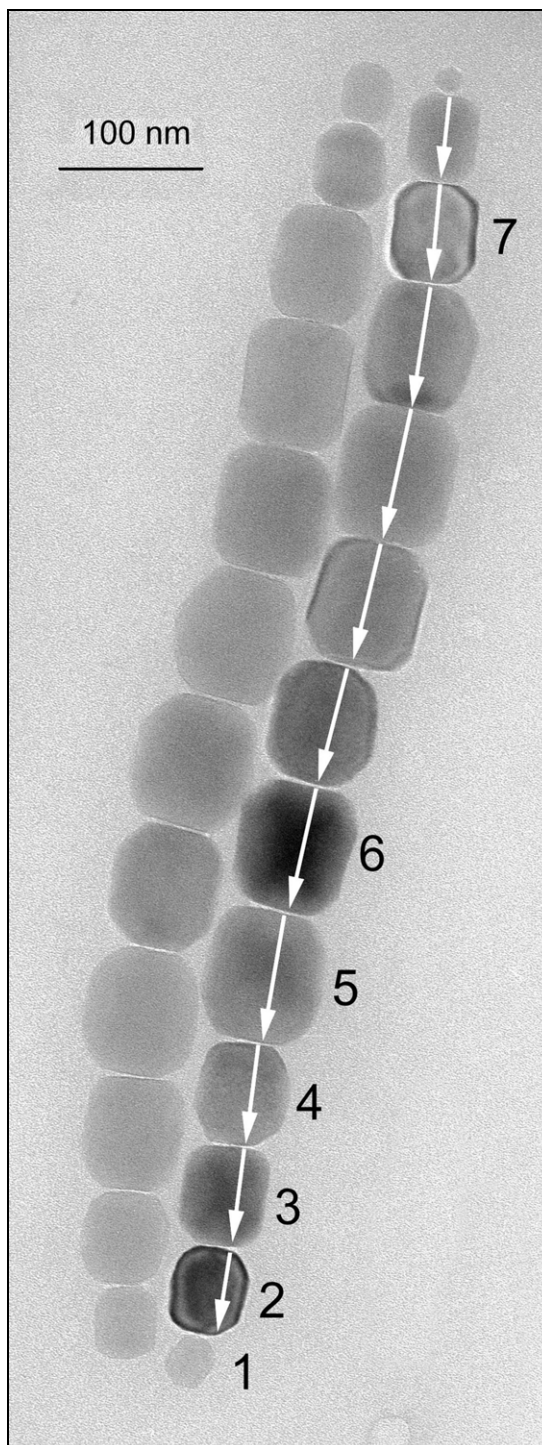
Figure 3. Bright-field image of a double chain of magnetite magnetosomes, acquired at 400 kV using a JEOL 4000EX TEM. The orientations of the crystals marked 1-7 are referred to in the text and in subsequent figures. The white arrows are approximately parallel to [111] in each crystal.
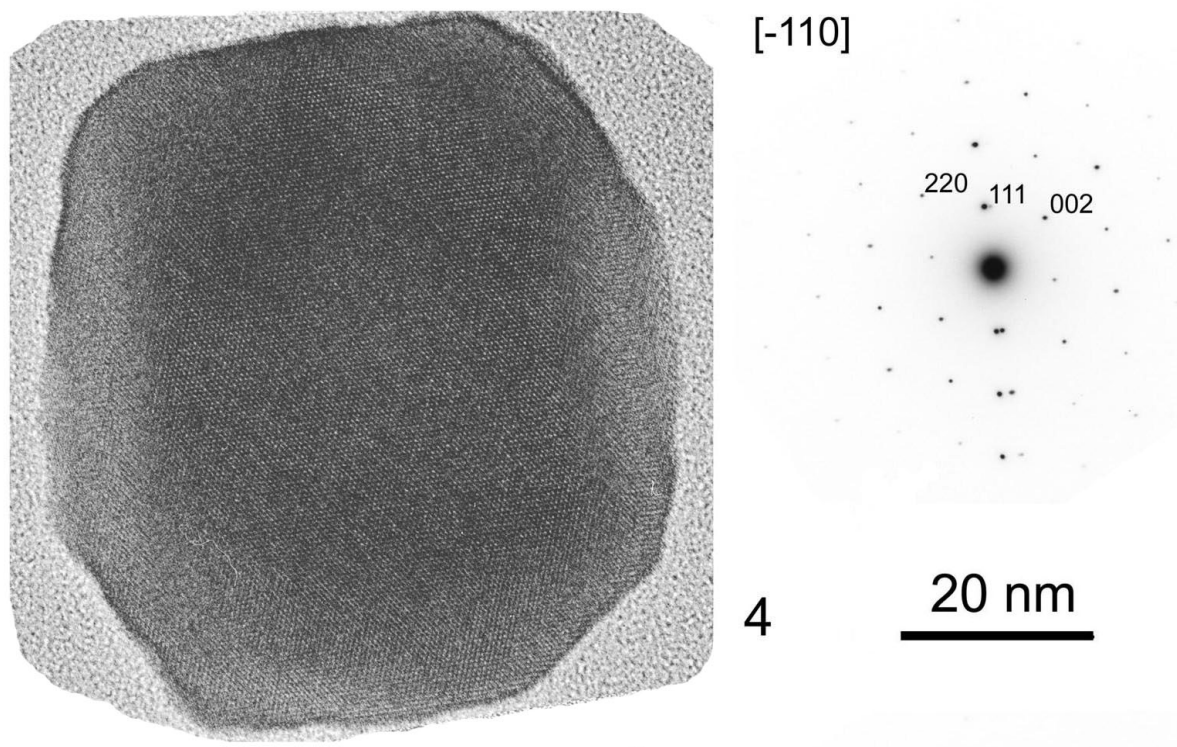
Figure 4. Zone axis HR image and SAED pattern acquired from crystal 4.
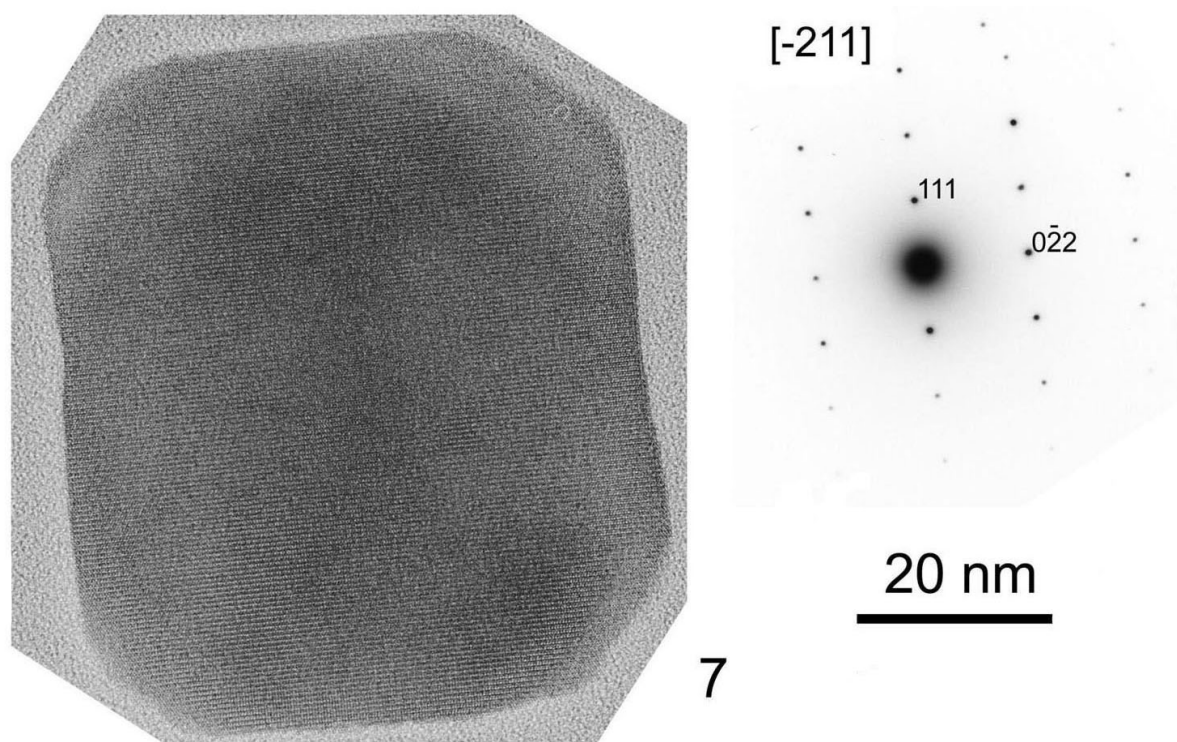
Figure 5. HR image and SAED pattern acquired from crystal 7.
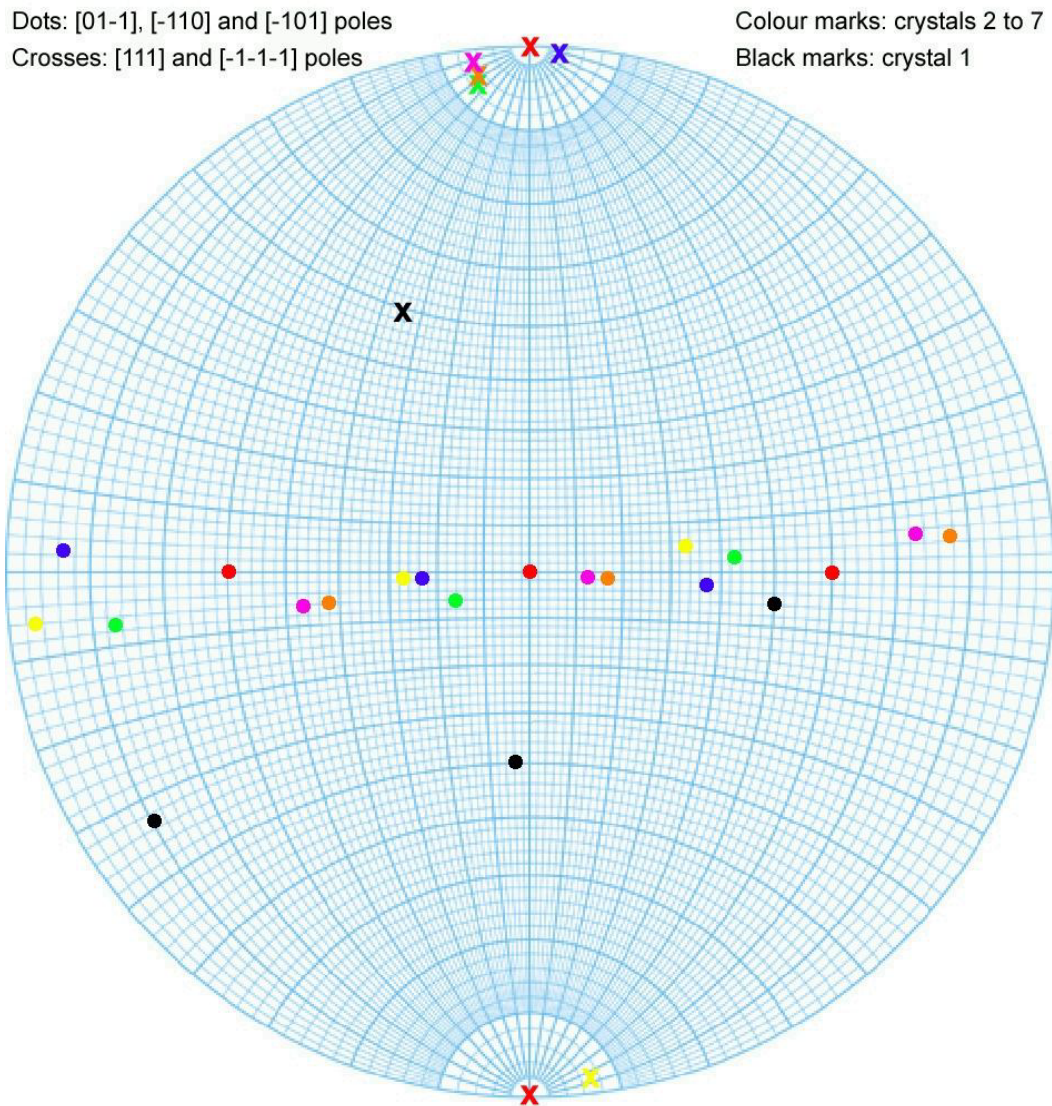
Figure 6. Stereogram of crystal orientations for the numbered crystals in the chain in figure 3. The crosses show the [111] poles which are all aligned in approximately the same direction (the direction of the chain axis), except for the black cross, corresponding to crystal 1 at the end of the chain. The dots show the <110> directions, which are more randomly distributed about the chain axis. Again, the directions associated with crystal 1 (in black) are not aligned close to the directions in crystals 2-7.

2.3 Off-axis electron holography

Magnetic induction maps of several magnetosome chains were obtained from off-axis electron holograms acquired at 300 kV using a Philips CM300-ST field emission gun (FEG) TEM equipped with a Lorentz lens, an electron biprism and a Gatan GIF 2000 imaging filter with a 2048 pixel charge coupled device (CCD) camera.

Figure 7 shows a schematic diagram of the electron-optical set-up of the microscope. The sample is illuminated coherently, with the region of interest positioned so that it covers approximately half the field of view. An electron biprism is used to overlap the electron wave that passes through the sample with a reference wave that passes only through vacuum, or alternatively through a thin region of clean support film. Interference of the two parts of the electron wave results in the formation of holographic fringes, which record both the amplitude and the phase shift of the electron wave that has passed through the sample. The Lorentz lens allows holograms of magnetic samples to be acquired at high magnification with the conventional microscope objective lens switched off, and with the sample in magnetic-field-free conditions. External magnetic fields can then be applied to the specimen by using the microscope objective lens to apply a field parallel to the optic axis of the microscope. The sample can be tilted to an angle of ~30° to provide a component of this external field in the plane of the sample. Details of the procedure used to record electron holograms, and to extract phase information from them, are described elsewhere [4].
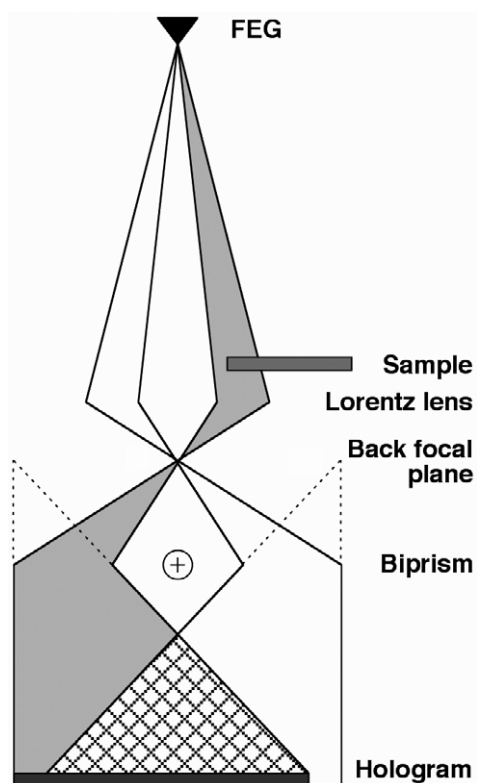
Figure 7. Schematic diagram showing the set-up for off-axis electron holography [4]. The FEG provides a coherent source of electrons. The Lorentz lens allows the sample to be examined in magnetic-field-free conditions. The biprism is used to form an electron hologram by overlapping an electron wave that has passed through the sample with another part of the same electron wave that has passed through vacuum.

The phase shift, ϕ, of the electron wave is affected by the magnetic induction, B, and the mean inner potential (MIP), V_0, according to the equations [4]:

$$\phi_{MIP} = C_E \int V_0 dz \qquad (1)$$

$$\phi_{mag} = \frac{e}{\hbar} \iint B dx dz \qquad (2)$$

where C_E is given by the expression

$$C_E = \frac{2\pi}{\lambda}\left(\frac{E + E_0}{E(E + 2E_0)}\right) \qquad (3)$$

In equations 1-3, E and E_0 are the kinetic and rest-mass energies of the incident electron, respectively, and z and x are directions parallel and perpendicular to the incident electron beam, respectively.

By magnetising the sample in opposite directions *in situ* in the electron microscope, acquiring electron holograms of these oppositely magnetised regions, and finally subtracting the resulting phase images from each other during processing, the MIP contribution to the phase shift can be eliminated, leaving only the magnetic signal of primary interest. Contours can then be generated from this magnetic phase image to produce a map of the in-plane component of the magnetic induction in the

sample [5,6]. The approach relies on being able to reverse the direction of magnetisation in the sample exactly. For chains of crystals this condition is likely to be met, and can be checked by repeating the same experiment several times. The approach also relies on diffraction contrast in the crystals being identical in each pair of images. Artefacts arising when this is not the case can usually be identified visually.

2.4. Off-axis electron holography of magnetite chains

Off-axis electron holograms of bacterial magnetite chains were recorded in magnetic-field-free conditions, both at room temperature and with the sample cooled using a double tilt liquid nitrogen cold holder. A thermocouple indicated that the cold holder nominally cooled the sample to 116 K, which is in the vicinity of the Verwey Transition (119 K), so we can be confident of being below the isotropic point of magnetite (130 K). However it was not possible to acquire diffraction patterns of the crystals to assess the true temperature of the crystals under the conditions used for electron holography. The present experiment can therefore be regarded as a preliminary study of the effect of temperature on magnetic microstructure in biogenic magnetite crystals.

Figure 8 shows a representative magnetic induction map of two double chains of magnetite crystals determined from holograms acquired at room temperature with the chains magnetised parallel and antiparallel to their length. The contours are highly constrained to be parallel to each other within the crystals and to follow the chain axis, although they deviate when breaks in the chain occur. Each chain is seen to behave relatively independently, however there is some transfer of magnetic flux between adjacent chains, as well as between the two pairs of chains in the figure.
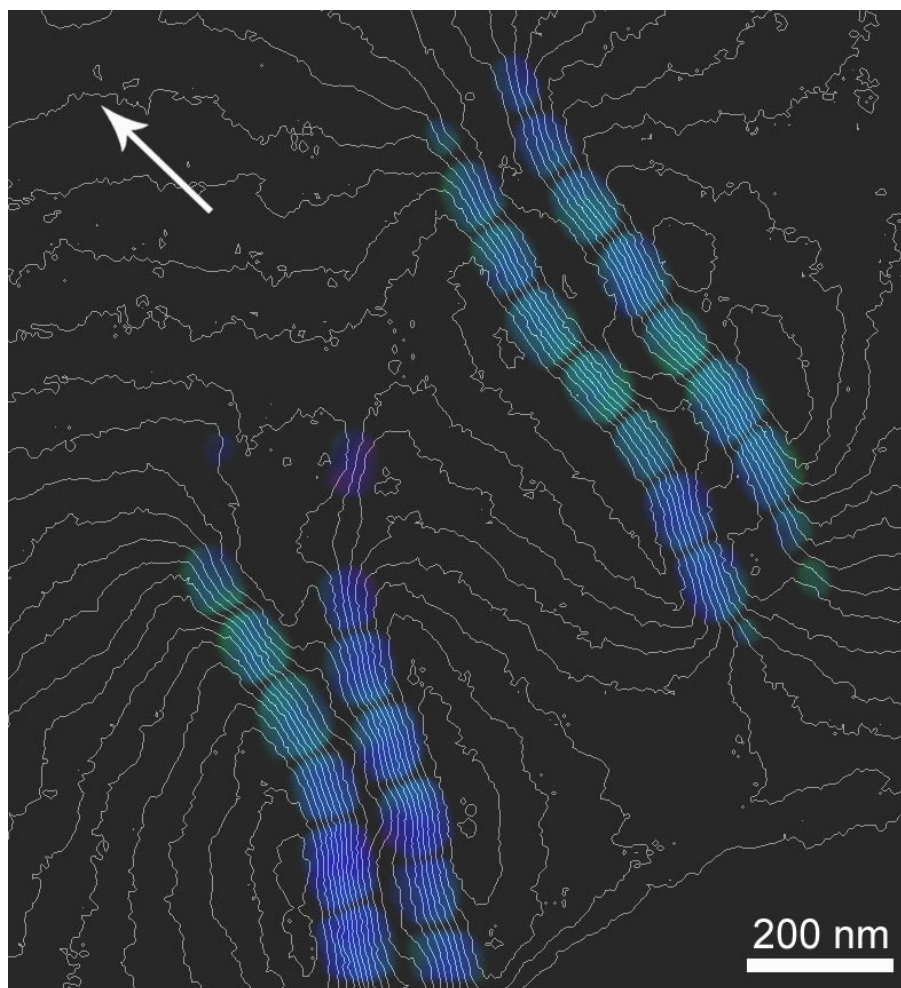
Figure 8. Magnetic phase contours measured using electron holography from two pairs of bacterial magnetite chains at 293 K, after magnetising the sample parallel and antiparallel to the direction of the white arrow. The colours, which were determined from the local gradient of the phase image, show the direction of the magnetic induction according to the colour wheel shown below. The contour spacing is 0.25 radians.

Figure 9 shows magnetic induction maps acquired from the same pairs of magnetite chains both at room temperature and at 116 K (close to the Verwey transition). Although the low-temperature induction map is noisier, as a result of sample drift limiting the acquisition time, a striking difference is apparent between the two images. Whereas the contours in the crystals are highly parallel to each other and to the chain axes at room temperature, their direction is far more variable and irregular at low temperature. This difference is most apparent in the colours that are used to represent the direction of the local magnetic induction in the crystals. For example, at low temperature some of the crystals in figure 9b show slightly S-shaped magnetic configurations. The return flux around each magnetite chain also appears to be better defined at room temperature than at low temperature. Although some of this difference may result from the increased noise in the low-temperature maps, it may also be associated with the greater variation in the magnetisation directions in the crystals, which therefore behave magnetically in a less collective manner. Similar behaviour is seen from two further pairs of magnetite crystals in figure 10.
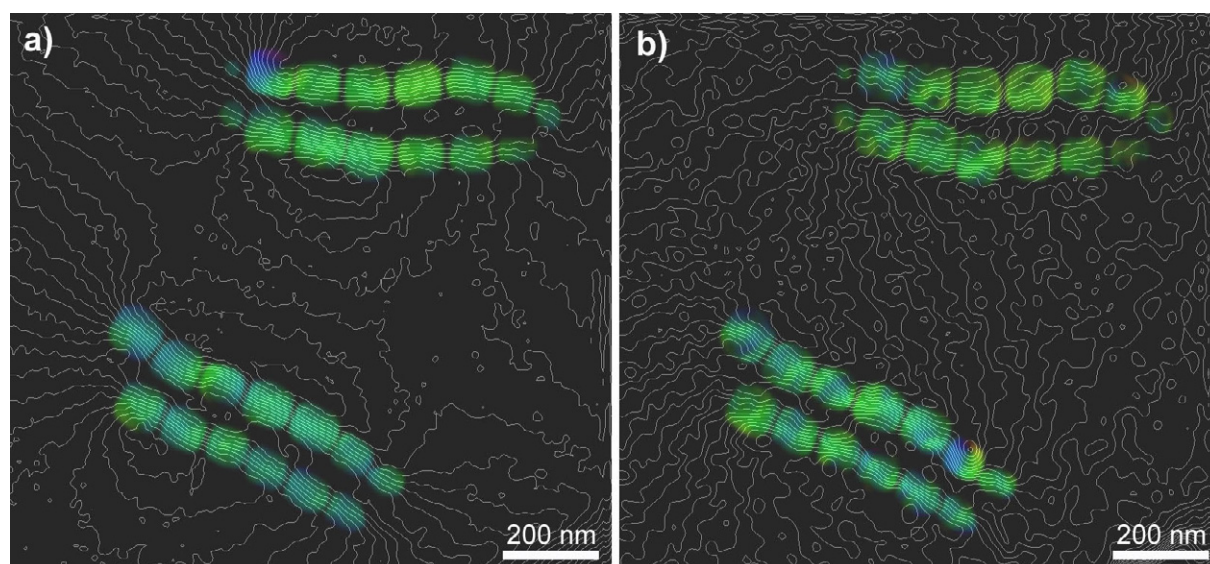
Figure 9. Magnetic induction maps acquired from two pairs of bacterial magnetite chains at a) 293 K and b) 116 K. In the room-temperature holograms, the contours are parallel to each other within the crystals and only deviate as a result of their morphologies and positions. At 116 K, this regularity is less evident. The field lines undulate to a greater degree within the crystals, as well as at kinks in the chains. The small vortex in the lower chain in b) is likely to be an artefact resulting from diffraction contrast in this crystal. The contour spacing is 0.25 radians in a) and 0.31 radians in b).

It was shown above that the chain axes in these bacteria are approximately parallel to the [111] directions of the magnetite crystals, which correspond to the crystallographic easy axis of magnetisation in magnetite at room temperature [7]. The change in structure from cubic to monoclinic at the Verwey transition is known to be associated with a change in the easy axis of magnetisation to an <001> direction of the original cubic structure [8]. Although particle interactions and shape anisotropy invariably result in the preservation of the overall magnetic induction direction along the chain axis at low temperature, it is likely that the undulation of the contours along the chain axes in the low-temperature holograms in figures 9 and 10 results from a competition between the effects of magnetocrystalline anisotropy, shape anisotropy and interactions, which are only mutually favourable at room temperature. Micromagnetic simulations will be used to assess the competition between these effects in a future study.
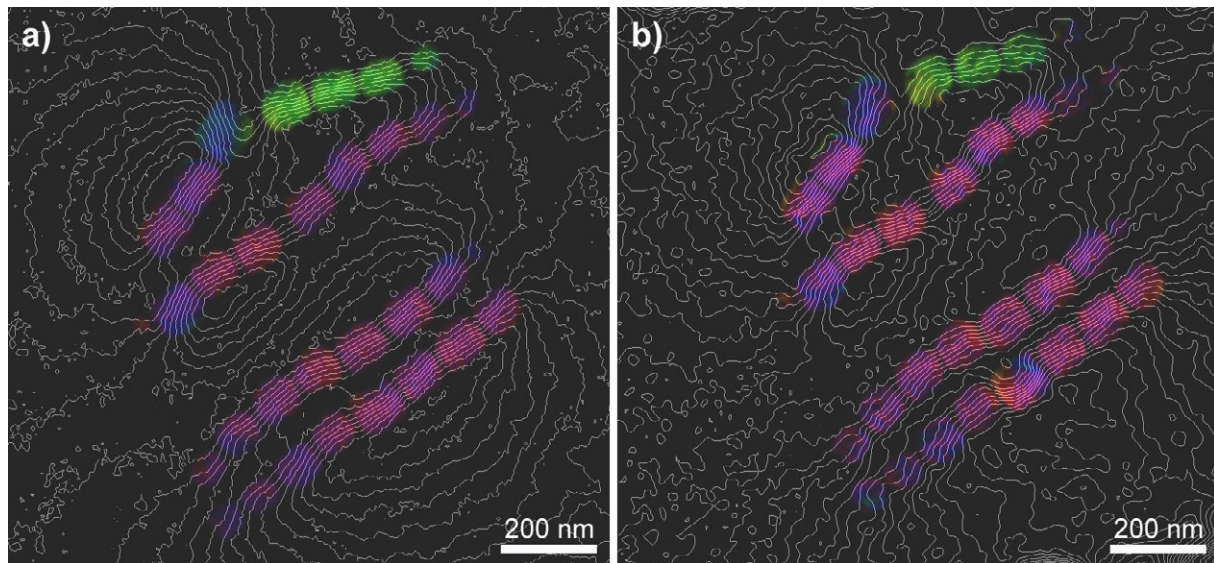
Figure 10. As for figure 9, but for a different bacterial cell. The map shown in a) was acquired at 293 K, and that in b) at 116 K. The large kink in the centre of the lower chain in b) is likely to be an artefact resulting from diffraction contrast. The contour spacing is 0.25 radians in both figures

It is interesting to examine the influence of the direction of the externally applied magnetic field on the magnetic microstructure in the magnetosome chains. In order to address this question, the region shown in figure 10 was examined at room temperature after applying both parallel and perpendicular fields to the chain. The difference in the resulting magnetic behaviour is shown in figure 11. In one of the pairs of chains, which are relatively straight, all of the particles are magnetised along the chain axes, irrespective of the applied field direction. In contrast, for a chain that is kinked, a large magnetic field applied perpendicular to the chain axis is able to split the chain into two oppositely magnetised segments. Although this behaviour is unlikely to be present naturally in living bacterial cells, it illustrates the large effect on the magnetic microstructure that can be introduced as a result of small disruptions in particle alignment along a chain.

2.5. The effect of temperature on magnetisation
Phase images acquired using electron holography can be used to measure the remanent magnetisation of the magnetite crystals quantitatively, which, for single domain crystals, is approximately equal to the saturation magnetisation. As mentioned above, a recorded phase image contains contributions from both the magnetic induction and the MIP of the sample. *In situ* reversal experiments allow the magnetic contribution to be separated from the total phase by taking half of the difference between phase images obtained for oppositely magnetised directions of the sample. Conversely, the MIP contribution to the phase shift can be obtained from half of the sum of these images, or equivalently by subtracting the magnetic contribution to the phase shift from the original phase images. In the absence of a stray (demagnetising) field, equations 1 and 2 can be reduced to

$$\phi_{MIP} = C_E V_0 t \tag{4}$$

$$\phi_{mag} = \frac{e}{\hbar} \int B t dx \tag{5}$$
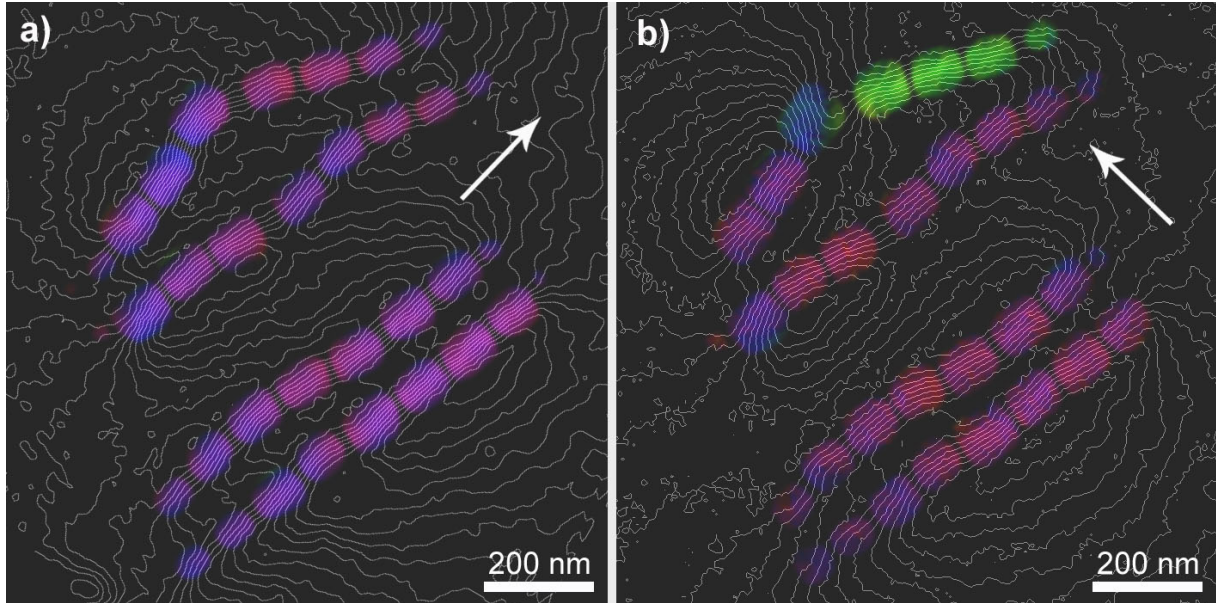
Figure 11. Illustration of the effect of changing the applied magnetic field direction on magnetic induction maps measured from two pairs of magnetite chains at 293 K. The applied field directions are indicated using white arrows. In a) the chains are magnetised in the same direction. In b) the top most chain is partially magnetised antiparallel to the other chains in the figure. As in previous figures, the different colours correspond to different magnetic induction directions.

By making use of equations 4 and 5, the specimen thickness, t, can be eliminated by evaluating the ratio

$$\frac{\phi_{MIP}}{\frac{d}{dx}\phi_{mag}} = \frac{\hbar C_E}{e} \frac{V_0}{B} \tag{6}$$

If a region of the sample is chosen in which demagnetising fields are negligible, such as a crystal in the centre of a chain of closely spaced magnetosomes, then the magnetic and MIP contributions to the phase shift can be used to measure the ratio V_0/B. This procedure is illustrated in figure 12 in the form of magnetic and MIP contributions to the phase shift of two pairs of magnetite chains (figures 12a and b) and line profiles generated from these images (figures 12c and d). The ratio given in equation 6 was measured for a large number of crystals both at room temperature and at low temperature. The results are plotted in the form of histograms in figure 13. The large scatter in the results is due to a combination of the effects of noise and diffraction contrast. Systematic errors resulting from the presence of demagnetising fields around the crystals are difficult to assess, but have been minimised by analysing only crystals close to the centres of the chains.

On the assumption that the MIP of magnetite does not change appreciably with temperature when compared with the change in magnetisation (the atomic scattering factors are not expected to vary with temperature significantly [9], and the change in density is negligible [10,11]), the magnetic induction can be determined from measurements of V_0/B if V_0 is known. Experimentally, the MIP of magnetite has been measured as 17 V [12].
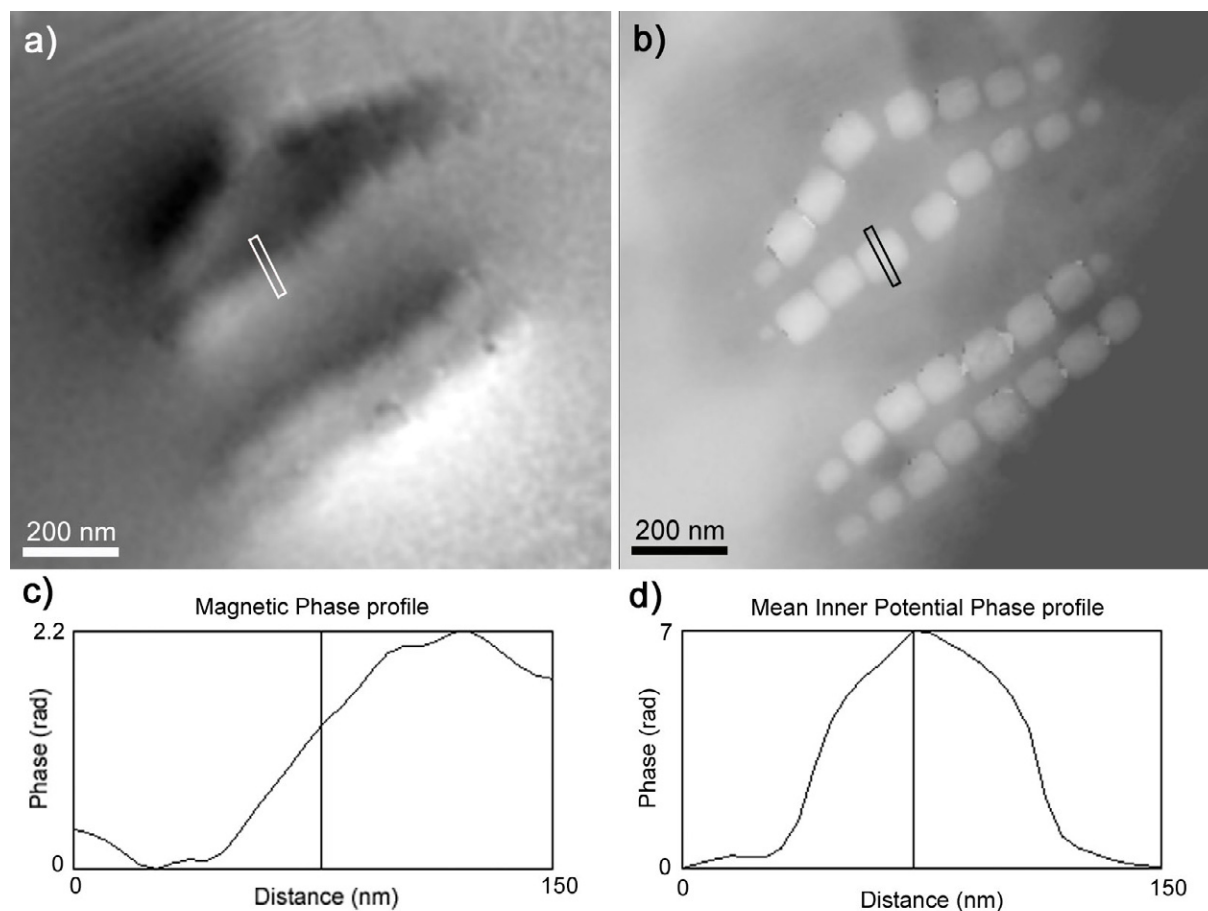
Figure 12. a) Magnetic and b) MIP contribution to the phase shift corresponding to figure 10b. Phase profiles from the indicated region are shown in c) and d). The derivative of the magnetic profile is used together with the MIP profile to measure V_0/B for each crystal in turn. Some phase unwrapping errors are visible in b).
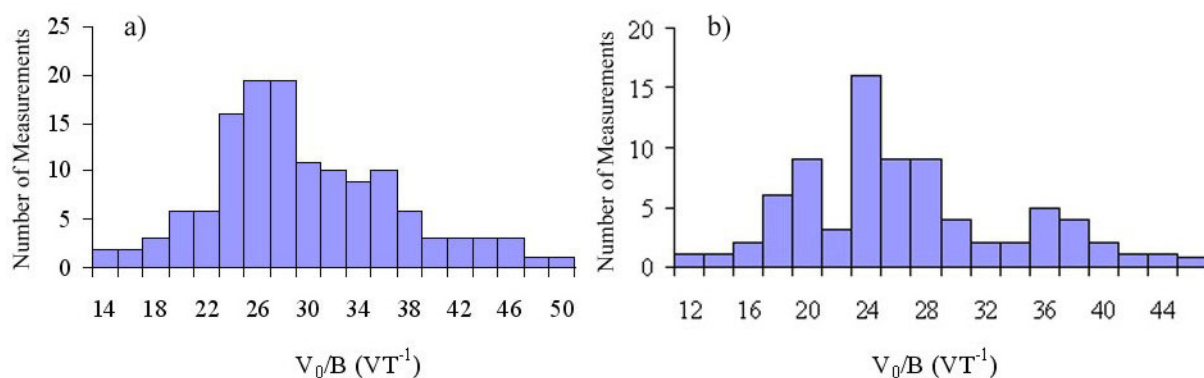
Figure 13. Histograms showing the measured V_0/B ratio for a large number of particles at a) 293 K and b) 116 K. The mean value of V_0/B, occurs at a) 29.5±0.8 VT^{-1} and b) 26.6±0.9 VT^{-1}.

Despite the scatter in the results shown in figure 13, the mean value of the measured magnetisation is seen to rise from 0.58±0.02 T at room temperature to 0.64±0.03 T at low temperature if a value of 17 V is assumed for the MIP of magnetite [12]. The error quoted in these measurements is the standard error in the mean, defined as

$$\sigma_m = \frac{\sigma}{\sqrt{n}} \tag{7}$$

where σ is the square root of the standard deviation and n is the number of measurements taken. The asymmetry in these results may arise due to demagnetising fields, and out of plane components of the field, both effects causing the measured value of B to be lower than the true value. This rise in magnetisation at low temperature is consistent with the behaviour of magnetite as reported in the literature, where room temperature magnetisation is 0.6 T, and the maximum value at lower temperatures is 0.63 T [7].

3. Conclusions
Off-axis electron holography and high-resolution electron microscopy have been used to examine the magnetic properties of bacterial magnetite chains at room temperature and close to the Verwey transition, and the relative orientations of the crystals. The competing effects of morphology, crystallography and interparticle interactions on the magnetic behaviour have been assessed experimentally. High-resolution electron microscopy has been used to show that the chains are crystallographically analogous to beads on a string, with their [111] directions constrained to lie parallel to the chain axis. This observation has implications for the magnetic properties of the crystals. At room temperature, with the easy axis parallel to the chain axis, the field lines are highly parallel. At lower temperature, with a magnetocrystalline easy axis that is no longer parallel to the chain axis, competition between the new easy axis of magnetisation, particle shape and interparticle interactions causes the magnetic field lines to undulate along the chain length. The quantitative nature of electron holography has been used to assess the change in the magnetisation of biogenic magnetite crystals with temperature, showing a rise from 0.58±0.02 T at room temperature to 0.64±0.03 T at a temperature close to the Verwey transition.

References
[1]   Bazylinski D A and Frankel R B 2004 Magnetosome formation in prokaryotes. *Nature Reviews Microbiology* **2(3)** 217-230
[2]   Verwey E J W 1939 Electronic conduction of magnetite (Fe_3O_4) and its transition point at low-temperature *Nature* **44** 327-328
[3]   Devouard B, Pósfai M, Hua X, Bazylinski D A, Frankel R B and Buseck P R 1998 Magnetite from magnetotactic bacteria: size distributions and twinning *Amer. Min.* **83** 1387-1399
[4]   Dunin-Borkowski R E, McCartney and Smith D J 2004 *Electron Holography of Nanostructured Materials (Encyclopedia of Nanoscience and Nanotechnology* vol 3) ed H S Nalwa (American Scientific Publishers) p 72,73
[5]   Dunin-Borkowski R E, McCartney M R, Pósfai M, Frankel R B, Bazylinski D A and Buseck P R 1998 Magnetic microstructure of magnetotactic bacteria by electron holography *Science* **282** 1868-1870
[6]   Dunin-Borkowski R E, McCartney M R, Pósfai M, Frankel R B, Bazylinski D A and Buseck P R 2001 Off-axis electron holography of magnetotactic bacteria: magnetic microstructures of strains MV-1 and MS-1 *Eur. J. Mineral* **13** 671-684
[7]   Özdemir Ö and Dunlop D J 1999 Low temperature properties of a single crystal of magnetite oriented along principal magnetic axes *Earth Planet. Sci. Lett.* **165** 229-239
[8]   Muxworthy A R and McClelland E 2000 Review of the low temperature magnetic properties of magnetite from a rock magnetic perspective *Geophys. J. Int.* **140** 101-114

[9]   Rez P 2004 Private communication

[10]   Dunlop D J and Özdemir Ö 1997 *Rock Magnetism: Fundamentals and Frontiers* (Cambridge University Press)

[11]   Iizumi M, Koetzle T F, Shirane G, Chikazumi S, Matsui M and Todo S 1982 Structure of magnetite (Fe_3O_4) below the Verwey transition temperature *Acta Cryst.* **B38**   2121-2133

[12]   Harrison R J, Dunin-Borkowski R E and Putnis A 2002 Direct imaging of nanoscale magnetic interactions in minerals *Proc. Nat. Acad. Sci.* **99** 16556-16561